Title

Disease-associated mutations in KCNE potassium channel subunits (MiRPs) reveal promiscuous disruption of multiple currents and conservation of mechanism.

Journal

FASEB journal : official publication of the Federation of American Societies for Experimental Biology, 16(3)

ISSN

0892-6638

Authors

Abbott, Geoffrey W

Goldstein, Steve AN

Publication Date

2002-03-01

DOI

10.1096/fj.01-0520hyp

Disease-associated mutations in KCNE potassium channel subunits (MiRPs) reveal promiscuous disruption of multiple currents and conservation of mechanism

GEOFFREY W. ABBOTT[1] AND STEVE A. N. GOLDSTEIN[2]

Departments of Pediatrics and Cellular and Molecular Physiology, Boyer Center for Molecular Medicine, Yale University School of Medicine, New Haven, Connecticut 06536 USA

ABSTRACT

KCNE genes encode single transmembrane-domain subunits, the MinK-related peptides (MiRPs), which assemble with pore-forming α subunits to establish the attributes of potassium channels in vivo. To investigate whether MinK, MiRP1, and MiRP2 operate similarly with their known native α subunit partners (KCNQ1, HERG, and Kv3.4, respectively) two conserved residues associated with human disease and influential in channel function were evaluated. As MiRPs assemble with a variety of α subunits in experimental cells and may do so in vivo, each peptide was also assessed with the other two a subunits. Inherited mutation of aspartate to asparagine (D → N) to yield D76N-MinK is linked to cardiac arrhythmia and deafness; the analogs D82N-MiRP1 and D90N-MiRP2 were studied. Mutation of arginine to histidine (R → H) to yield R83H-MiRP2 is associated with periodic paralysis; the analogs K69H-MinK and K75H-MiRP1 were also studied. Macroscopic and single-channel currents showed that D → N mutations suppressed a subset of functions whereas R/K → H changes altered the activity of MinK, MiRP1, and MiRP2 with all three a subunits. The findings indicate that the KCNE peptides interact similarly with different a subunits and suggest a hypothesis: that clinical manifestations of inherited KCNE point mutations result from disruption of multiple native currents via promiscuous interactions.— Abbott, G. W., Goldstein, S. A. N. Disease-associated mutations in KCNE potassium channel subunits (MiRPs) reveal promiscuous disruption of multiple currents and conservation of mechanism. FASEB J. 16, 390 – 400 (2002)

Key Words: MinK · MiRP1 · MiRP2 · KCNQ1 · HERG · Kv3.4 · periodic paralysis · cardiac arrhythmia

Classical voltage-gated potassium channels contain four pore-forming (α) subunits that supply domains that sense and respond to voltage and mediate ion permeation (1). In native cells, potassium channels incorporate additional subunits that modify attributes as varied as surface half-life, ion selectivity, gating kinetics, chemical and secondary messenger regulation, and pharmacology (2). Subunits encoded by KCNE genes are single transmembrane-domain peptides that assemble with α subunits to influence all these functional parameters (3). Thus, the KCNE1 product MinK (4) partners with the α subunit KCNQ1 to form the slowly activating cardiac current I_{Ks} found in heart and ear (5, 6). Similarly, the KCNE2 product MinK-related peptide 1 (MiRP1) assembles with the α subunit HERG to generate a current resembling cardiac I_{Kr} (7) and the KCNE3 product MiRP2 combines with the Kv3.4 α subunit to form a subthreshold, A-type channel in skeletal muscle (8). Inherited mutations in MinK are associated with cardiac arrhythmia and deafness (9 – 12), those in MiRP1 with inherited and drug-induced cardiac arrhythmia (7, 13), and those in MiRP2 have been linked to periodic paralysis (8).

These recognized MiRP/α subunit partnerships may not be unique. In experimental cells, MinK has been found to assemble not only with KCNQ1 (5, 6) but also with HERG (14); MiRP1 combines not only with HERG (7, 15), but with Kv4.2 (16, 17) and perhaps HCN1 (18); and MiRP2 associates not only with Kv3.4 (8) but with KCNQ1 and HERG (19, 20). Whereas such observations suggest that α subunits in native cells may rarely function alone (21), these varied partnerships have not yet been demonstrated in vivo.

The idea that KCNE peptides can alter the function of more than one α subunit type suggests they might operate in different complexes in similar fashion, presumably via common subunit-subunit

[1] Present address: Cardiology Division, Departments of Medicine and Pharmacology, Weill Medical College of Cornell University, New York, NY 10021, USA.

[2] Correspondence: Section of Developmental Biology and Biophysics, 295 Congress Ave., New Haven, CT 06536, USA. E-mail: steve.goldstein@yale.edu

interactions. To explore this notion, we studied two residues essential to MinK and MiRP2 function and strongly conserved in the five known MiRPs: D76N-MinK was recognized by its association with inherited arrhythmia and deafness and alters function of channels formed with KCNQ1; an equivalent aspartate (D) is present in all but MiRP3 (2, 9, 12, 22). R83H-MiRP2 was identified by its sway over channels formed with Kv3.4 and association with periodic paralysis; an homologous arginine (R) or lysine (K) is found in all five MiRPs (2, 3, 8). Here, despite changes at these conserved sites in MinK, MiRP1, and MiRP2, each peptide retained the capacity to form functional complexes with its α subunit partners (KCNQ1, HERG, and Kv3.4); conversely, D → N changes eliminated MiRP-mediated current up-regulation (but not down-regulation) and R/K → H mutations suppressed effects on current activation, deactivation, and magnitude, suggesting this residue may have a key role in activity. The findings demonstrate that many MiRP/α subunit operations do proceed by shared mechanisms. The results suggest a hypothesis for how a single KCNE point mutation might cause disease—through effects on more than one α subunit channel type in vivo.

MATERIALS AND METHODS

Heterologous expression

Mutations were produced in wild-type human KCNE2 and KCNE3 in pGA1 (7) or wild-type human KCNE1 (Ser38 variant) in pRAT (23) by pfu-based mutagenesis (Quick-Change Kit; Stratagene, La Jolla, CA), followed by insertion of mutant gene fragments into translationally silent restriction sites and confirmed by DNA sequencing. For studies in oocytes, cRNA was produced as before (7). Chinese hamster ovary (CHO) cells were treated with Superfect (Qiagen, Chatsworth, CA) and plasmids carrying the genes for MIRP2, Kv3.4, and green fluorescent protein were expressed in pCI neo-based vectors (Promega, Madison, WI), as before (8).

Electrophysiology

CHO cells

Kv3.4 and MiRP2-Kv3.4 channels were assessed using CHO cells by whole-cell or patch clamp 1–3 days after transfection. Recording was with an Axopatch 200A Amplifier (Axon Instruments, Foster City, CA), an IBM computer, and CLAMPEX software (Axon). Data analysis was performed using CLAMPFIT, FETCHAN, PSTAT (Axon), and TAC
software (Instrutech, Great Neck, NY).

Oocytes

HERG, KCNQ1, or Kv3.4 channels with and without MinK, MiRP1, or MiRP2 were assessed using *Xenopus laevis* oocytes and two-electrode voltage clamp (TEVC), as before (7). Resting membrane potential (RMP) of oocytes was assessed at steady state in current clamp. All experiments were performed at room temperature. Oocytes were used for most subunit partnerships. MiRP2/Kv3.4 channels were usually studied in CHO cells, as regulatory influences maintain stable current levels over the course of measurements (not shown). That MiRP2/Kv3.4 complexes do assemble in oocytes is shown by altered affinity of BDS-II here and earlier (8). Such cell-specific effects of KCNE peptides on current density and pharmacology are not without precedent; see refs 14, 24 for differential effects of D76N-minK on HERG and (7) for altered E-4031 blockade, respectively. For BDS-II blockade, CHO cell recordings were performed using outside-out patches, oocyte recordings using whole-cell TEVC; BDS-II was applied via a bath in both cases.

Protocols

Holding voltage was -80 mV unless stated otherwise. 1: Peak patch current; 3 s pulse from -100 to 90 mV in 10 mV steps with a 10 s interpulse interval. 2: Single voltage/drug inhibition; repetitive 3 s pulses to a single voltage as indicated with a 5 s interpulse interval. 3: Steady state; holding at -40 mV for 5–20 min with no interpulse interval. 4: Peak whole-cell current; 3 s pulse from -120 to 60 mV in 20 mV steps, followed by a 1.5 s tail pulse to -30 mV, with a 10 s interpulse interval. 5: Peak whole-cell current (MinK); 5 s pulse from -80 to 60 mV in 20 mV steps with a 10 s interpulse interval. 6: Steady-state activation; 3 s prepulse from -80 to 60 mV in 20 mV steps, followed by a 3 s pulse to -30 mV, with a 10 s interpulse interval. 7: Peak tail current/deactivation kinetics; 3 s prepulse to 40 mV, followed by a 3 s pulse from -120 to 60 mV in 20 mV steps with a 10 s interpulse interval.

Ionic conditions

Pipette solution for CHO cells in on-cell mode was (in mM): 100 KCl, 0.7 $MgCl_2$, 1 $CaCl_2$, 10 HEPES pH 7.4. CHO cell bath solution was as in the pipette. Bath solution for oocytes was (in mM) 4 KCl, 96 NaCl, 0.7 $MgCl_2$, 1 $CaCl_2$, 10 HEPES pH 7.4; for RMP measurements, KCl was varied from 0.01 to 100 mM, with NaCl being substituted to keep the total monovalent ion concentration at 100 mM.

RESULTS

A conserved KCNE site influential in both MinK/KCNQ1 and MiRP2/Kv3.4 channels

MinK assembles with KCNQ1 to slow channel activation, alter the voltage dependence of gating, and increase unitary conductance, thereby producing the attributes of native I_{Ks} channels (5, 6). Aspartate (D) to asparagine (N) mutation to yield D76N-MinK is associated with inherited long QT syndrome, sudden death, and deafness (9 –11). Compared with wild-type MinK/ KCNQ1 channels, the mutant reduces current density due to a shift of voltage-dependent activation to more positive potentials and a fourfold reduction in unitary conductance (9, 12). Sequence alignment of MinK, MiRP1, and MiRP2 indicates that D76-MinK is a conserved residue (Fig. 1); a homologous D is also present in MiRP4 but not MiRP3 (3). To assess whether this site was significant to MiRP2 function, D90N-MiRP2 was produced and studied with its skeletal muscle partner Kv3.4.

Wild-type MiRP2 shifts the voltage dependence of channels formed with Kv3.4 to more negative potentials (change ~ -45 mV) to create a channel that activates at subthreshold levels and has an increased unitary conductance (8). Compared with wild-type MiRP2/ Kv3.4 channels, expression of D90N-MiRP2 reduced outward current density 3- to 4-fold (345±84 and 90±12 pA at 90 mV, respectively, *n*=9 –11 patches) and diminished inward currents 18-fold (-91±35 and -4.7±1.2 pA, respectively, at -50 mV) using CHO cells, on-cell patches, and ~ symmetrical potassium across the membrane (Fig. 2A, B). The mutation produced a +35 mV change in the midpoint activation potential ($V_{1/2}$) from -38 ± 1.0 to 2.8 ± 3.7 mV (Fig. 2C), similar to the value of Kv3.4 channels without MiRP2 (8).

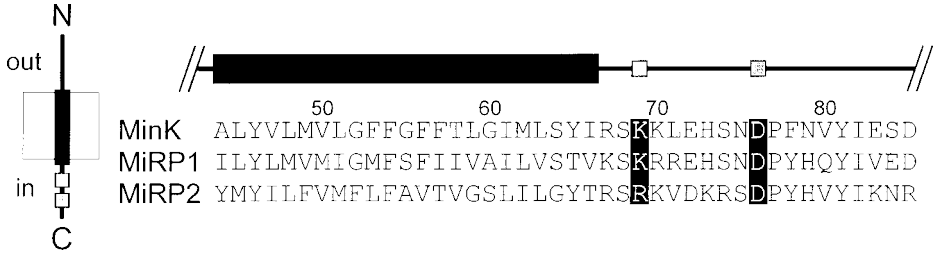

Figure 1. Partial sequence and predicted topology of KCNE-encoded, MinK-related peptides (MiRPs). Predicted topology (left) and partial sequences (right) of human MinK, MiRP1, and MiRP2 indicating extracellular (out) N and intracellular (in) C termini; alignment with numbering for MinK shows part of the predicted transmembrane (thick line) and membrane-following region (thin line) with sites studied boxed in black: K69H (MinK); K75H (MiRP1); R83H (MiRP2) [open square]; D76N (MinK); D82N (MiRP1); D90N (MiRP2) [gray square].

Whenever KCNE mutation yielded attributes like those for channels formed by α subunits alone, we sought evidence to confirm that the altered peptides were assembled into the channel complex. Two observations with macroscopic currents indicated that channels did contain D90N-MiRP2 subunits. First, the slope of the conductance-voltage relationship with D90N-MiRP2 was similar to that for wild-type MiRP2 (13±2.0 and 14±1.4, respectively) rather than that for homomeric Kv3.4 channels (22.5±0.6) (Fig. 2C). Second, channels with D90N-MiRP2 were blocked by the peptide toxin BDS-II like those containing wild-type MiRP2 (K_i=633±110 and 688±166 nM at+30 mV, respectively, *n*=4 –5 cells), and significantly different from channels formed with Kv3.4 subunits alone, which showed ~sixfold greater sensitivity to the toxin (99.5±32 nM) (Fig. 2D)

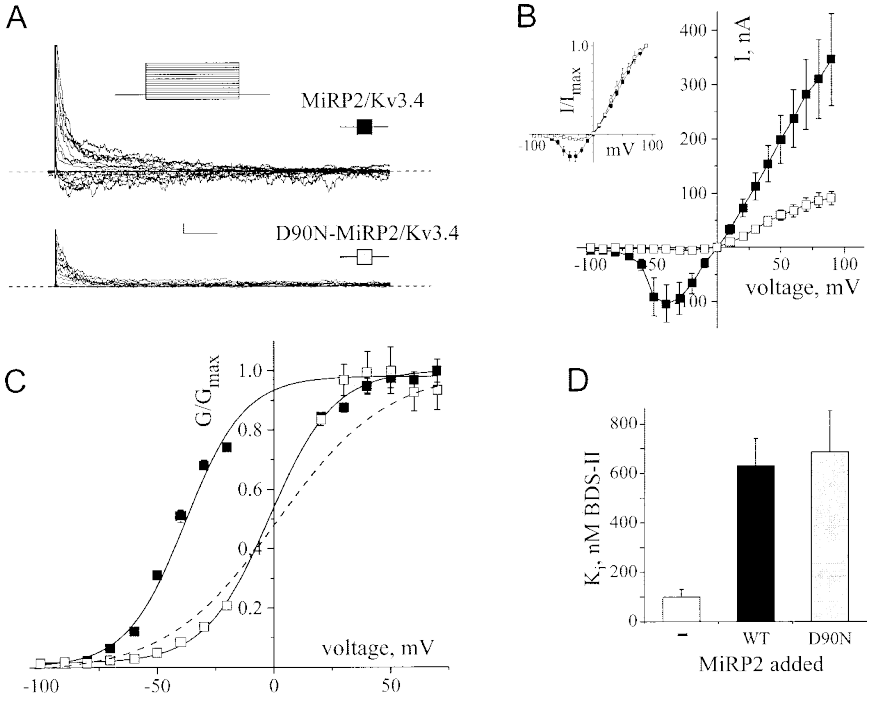

Figure 2. D90N-MiRP2/Kv3.4 channels show altered voltage dependence and reduced potassium flux. Studies of wild-type MiRP2/ Kv3.4 (black squares), D90N-MiRP2/Kv3.4 (gray squares), and Kv3.4 (dashed line) performed in CHO cells in on-cell patches with 100 mM potassium solution in bath and pipette using protocol 1. Sampled at 5 kHz, filtered at 1 kHz or 500 Hz. A) Representative current families in patches with high channel density; holding voltage -80 mV, steps from -100 to 90 mV (inset, protocol 1); scale bars 20 pA and 100 ms; zero current level (dashed line). B) Peak current-voltage relationship for recordings as in panel A. Mean ± se, *n* = 9 –11 patches; inset, normalized current-voltage relationship. C) Normalized conductance-voltage relationship for panel B. Curves fit to a function of the form: $1/\{1+\exp[(V_{1/2}- V)/V_s]\}$, where $V_{1/2}$ is the half-maximal voltage of activation and Vs the slope factor; values in text.; error bars indicate se. Dashed line shows results for homomeric Kv3.4 channels as reported (8). D) Blockade by BDS-II. Dose-response curves using Xenopus oocytes and protocol 2. Various levels of BDS-II applied in the bath with 4 mM potassium solution. Bars indicate equilibrium inhibition constant calculated from fits to the function: $y = [A_1-A_2/\{1+(x/x_o)^p\}]+A_2$, where x is added toxin, x_o the inhibition constant, and p the Hill coefficient. Mean ± se for 4 –5 oocytes. Kv3.4 (open); wild-type MiRP2/Kv3.4 (black); D90N-MiRP2/Kv3.4 (gray).

At the single-channel level, the effects of D76N-MinK on KCNQ1 and D90N-MiRP2 on Kv3.4 were also similar (Fig. 3). 1) D90N-MiRP2 produced a shift in activation voltage such that openings were rare and short-lived at voltages negative to -20 mV (Fig. 3A). 2) Mean unitary current amplitude was lowered by D90N-MiRP2 (Fig. 3B, C). Thus, wild-type MiRP2/Kv3.4 single channels showed two current amplitude levels (Fig. 3B, 1.5±0.1 and 2.2±0.1 pA at 60 mV) whereas D90N-MiRP2/Kv3.4 channels showed a single level similar in magnitude to the lower wild-type current level (Fig. 3B, 1.6±0.1 pA at 60 mV), similar to channels with Kv3.4 subunits alone (8). 3) Analysis of channel gating kinetics revealed that steady-state open probability (Po) at -40 mV for channels with D90N-MiRP2 was ~10-fold lower than for wild-type

MiRP2/Kv3.4 channels, P_o = 0.0040 ± 0.0004 and 0.04 ± 0.10, respectively, *n* = 3–5 patches (Fig. 3D, E, upper). Both wild-type and D90N-MiRP2 channels showed two open state dwell times (Fig. 3E lower); D90N mutation led to shortening of both dwell times and preferential occupancy of the shorter open state. Thus, dwell-time analysis for D90N-MiRP2/Kv3.4 channels suggested open dwell times with time constants (τ) of 0.7 ± 0.3 and 3.9 ± 0.3 ms (weights of 0.37±0.1 and 0.63±0.1, respectively) vs. wild-type MiRP2/Kv3.4 channels (τ = 1.80±0.03 and 21.0±0.1 ms, weights of 0.49±0.03 and 0.51±0.04, Fig. 3E, lower). Although dwell-time statistics for D90N-MiRP2/Kv3.4 channels should be treated with caution due to infrequent openings at this voltage, incorporation of the mutant into the complex was readily appreciated because single Kv3.4 channels demonstrate short-lived dwell times best fit to just a single exponential, as reported (τ = 2.60±0.06 ms) (8).

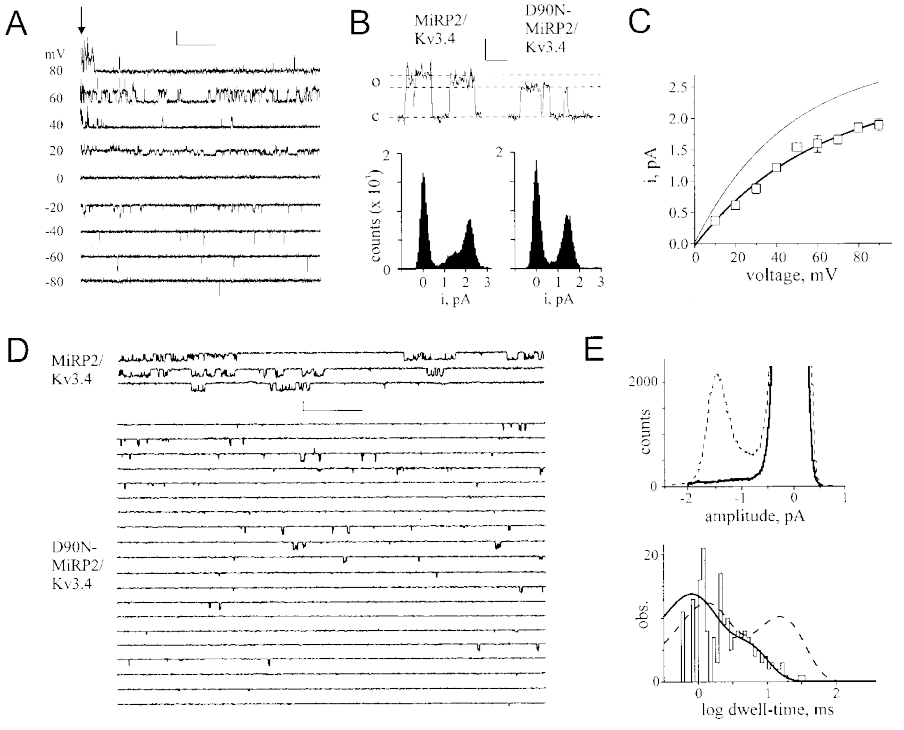

Figure 3. D90N-MiRP2/Kv3.4 channels show lower unitary current and open probability. Studies of single wild-type MiRP2/Kv3.4 or D90N-MiRP2/ Kv3.4 channels expressed in CHO cells with on-cell-attached patches and 100 mM potassium solution in bath and pipette. Sampled at 5 kHz, filtered at 1 kHz for analysis, and 500 Hz for presentation. A) Activation (arrow) of ~5 D90N-MiRP2/Kv3.4 channels by steps from a holding voltage of -80 mV according to protocol 1. Scale bars, 2 pA and 500 ms. B) Upper panel: single-channel openings at 60 mV for wild-type MiRP2/Kv3.4 (left) or D90N-MiRP2/ Kv3.4 (right). Scale bars represent 1 pA and 50 ms. Dashed lines at open state levels: o, open; c, closed. Lower panel: all-points histograms for openings at 60 mV for wild-type MiRP2/Kv3.4 (left) or D90N-MiRP2/Kv3.4 (right) channels; mean current levels in text. C) Unitary current-voltage relationship calculated from all-points histograms as in panel B for wild-type MiRP2/Kv3.4 (thin line, ref 8) and D90N-MiRP2/Kv3.4 (gray squares), mean ± $_{SE}$ for 3–9 patches per point. D) Single-channel steady-state currents; scale bars 1 pA and 500 ms (protocol 3). Representative traces (6 s per line) are continuous and taken from 5–10 min records. Top: wild-type MiRP2/Kv3.4; bottom: D90N-MiRP2/Kv3.4. E) Upper panel: all-points histograms from steady-state wild-type MiRP2/Kv3.4 (dashed) and D90N-MiRP2/Kv3.4 (solid line) single-channels held at -40 mV for 5–10 min and indicative of P_o. Lower panel: dwell-time histogram at -40 mV from single D90N-MiRP2/Kv3.4 channels held at steady state for 5–10 min; fit to a double exponential function (solid line) using Marquardt least-squares (PSTAT). A double exponential function dwell-time fit for single wild-type MiRP2/Kv3.4 channels is shown for comparison (dashed line). Wild-type fits as reported (8); τ values in text.

KCNQ1 is similarly affected by D76N-MinK and D90N-MiRP2

Whereas MinK is the 'classical' partner for KCNQ1 (5, 6), expression of MiRP2 with KCNQ1 in experimental cells produces a potassium-selective, voltage-insensitive (leak-type) current (Fig. 4A), as

others have shown (20). Here we report that D90N-MiRP2 acts like D76N-MinK to alter the voltage dependence and decrease macroscopic current passed by KCNQ1-containing channels. Compared with wild-type MiRP2, D90N-MiRP2 decreased macroscopic current density ~four-fold: mean current at 40 mV was 1.9 ± 0.2 μA for channels with D90N-MiRP2 vs. 7.3 ± 0.4 μA for wild-type MiRP2/KCNQ1 channels. Homomeric channels with KCNQ1 alone passed 4.6 ± 0.4 μA under the same conditions (Fig. 4B, *n* = 18-24 cells). Furthermore, D90N-MiRP2 restored time and voltage dependence to MiRP2/KCNQ1 currents. Thus, wild-type MiRP2/ KCNQ1 channels displayed a linear current-voltage relationship from -120 to +60 mV whereas D90N-MiRP2/KCNQ1 channels were well fitted to a Boltzmann function with a $V_{1/2}$ of -9 ± 3 mV and slope of 24 ± 2, more similar to KCNQ1 channels ($V_{1/2}$ = 1 ± 3 mV, slope = 23 ± 3) (Fig. 4B).

The D90N-MiRP2 subunit also acted to decrease the influence of MiRP2/KCNQ1 channels on RMP. The RMP of oocytes expressing only wild-type MiRP2 was not significantly different from control cells whereas expression of MiRP2 and KCNQ1 produced a shift of -72 ± 3 mV, D90N-MiRP2 and KCNQ1 a shift of -36 ± 7 mV, and KCNQ1 alone a -22 ± 2 mV change when evaluated with a low potassium bath solution (Fig. 4C).

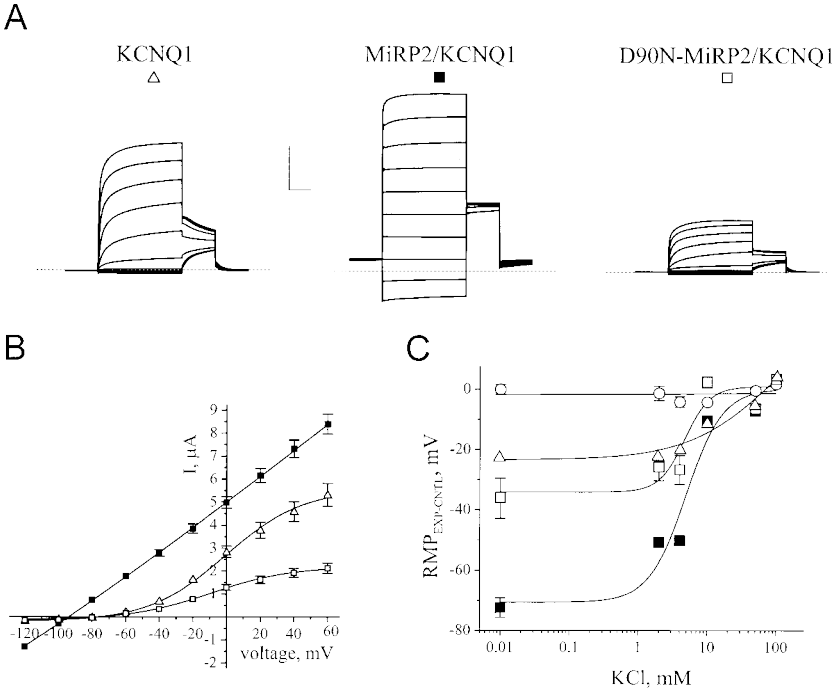

Figure 4. D90N-MiRP2/KCNQ1 channels show reduced current density and recovery of voltage and time dependence. Channels with KCNQ1 (triangle), wild-type MiRP2/ KCNQ1 (filled squares), or D90N-MiRP2/ KCNQ1 (gray squares) in oocytes by two-electrode voltage clamp. A) Representative currents recorded with protocol 1 in oocytes and 4 mM potassium solution in the bath. Dashed line indicates zero current level; scale bars, 2 μA and 1 s. B) Current-voltage relationships for cells as in panel A; mean ± se for 18 –24 oocytes. Wild-type MiRP2/ Kv3.4 fit with a straight line; Kv3.4 and D90N-MiRP2/Kv3.4 fit to a function of the form: $1/\{1+\exp[(V_{1/2}-V)/V_s]\}$, where $V_{1/2}$ is the half-maximal voltage of activation and V_s the slope factor. C) Change in mean resting membrane potential from control ($RMP_{Expt-Cntl}$) for various concentrations of bath potassium. Oocytes with wild-type MiRP2 alone (open circle) did not differ from control. Values are in text. Mean ± $_{SE}$ for 5–10 oocytes.

R83H-MiRP2 affects KCNQ1 and Kv3.4 similarly

MiRP2 assembles with Kv3.4 to form a potassium channel active at subthreshold potentials that influences skeletal muscle cell RMP; the missense mutant R83H-MiRP2 is associated with an inherited periodic paralysis; compared with wild-type MiRP2, the mutant reduces currents and causes skeletal muscle cell depolarization (8). Three effects of the mutation on Kv3.4-containing channels are described here.

1) The R83H variant altered voltage dependence of gating, producing a shift in the $V_{1/2}$ for activation

of ~ +30 mV to -9.2 ± 2.1 mV (Fig. 5A, B); this remains ~ 10 mV more negative than the $V_{1/2}$ of homomeric Kv3.4 channels (Fig. 2C). The slope conductance for R83H-MiRP2/Kv3.4 currents was 19 ± 2.2 mV (n=9 patches), intermediate between that of D90N-MiRP2/ Kv3.4 and wild-type MiRP2/Kv3.4 channels (Fig. 5B). 2) At the single-channel level, R83H-MiRP2/Kv3.4 currents were of slightly smaller amplitude than wild-type and displayed fewer openings at negative potentials (Fig. 5C, D). Thus, R83H-MiRP2/Kv3.4 channels exhibited two open states (like wild-type), but the larger current measured just 1.8 ± 0.2 pA at 60 mV (n=5) vs. 2.2 ± 0.1 pA for wild-type (Fig. 3B). 3) Steady-state open probability (P_o) at -40 mV for channels with R83H-MiRP2 was 0.006 ± 0.002 (n=11 patches), ~10-fold lower than for wild-type MiRP2/Kv3.4 channels but 12-fold more active than homomeric Kv3.4 channels (Fig. 5E, F). Although channels with R83H-MiRP2 showed two open state dwell times like wild-type (Fig. 5F, lower), the mutation shortened both dwell times and favored occupancy of the shorter opening. Thus, R83H-MiRP2/Kv3.4 had open state time constants (τ) of 0.48 ± 0.2 and 9.8 ± 0.2 ms (weights of 0.78 ± 0.2 and 0.22 ± 0.03, respectively), values intermediate between those of D90N-MiRP2/Kv3.4 and wild-type MiRP2/ Kv3.4 channels (Fig. 3E). We previously showed that the effects of the R83H mutation were not due to altered subunit assembly as R83H-MiRP2/Kv3.4 channels in excised CHO cell patches were blocked by BDS-II (like those with wild-type MiRP2) and ~ 20-fold less effectively than homomeric Kv3.4 channels (8).

The effects of R83H-MiRP2 on KCNQ1 were similar to those of D90N-MiRP2 although less potent (Fig. 6). Like channels with wild-type MiRP2, R83H-MiRP2/ KCNQ1 exhibited a largely linear current-voltage relationship; however, the mutation restored some time and voltage dependence to channel activation and decreased macroscopic currents (Fig. 6A, B). Flux was decreased ~twofold from 7.3 ± 0.4 μA for channels with wild-type MiRP2 to 4.3 ± 0.3 μA for channels with R83H-MiRP2 (Fig. 6B), similar to what is seen with homomeric KCNQ1 channels (Fig. 4B). As a result, the RMP of R83H-MiRP2/KCNQ1-expressing cells was shifted by +15 ± 7 mV in comparison to those with wild-type MiRP2/KCNQ1 channels (Fig. 6B, inset). Confirmation that R83H-MiRP2 subunits remained competent to assemble with KCNQ1 was afforded by clotrimazole, which blocked homomeric KCNQ1 channels less effectively (K_i = 419±22 μM) than either those with wild-type or R83H-MiRP2 (K_i= 217±20 and 177±18 μM, respectively) (Fig. 6C).

K69H-MinK also alters KCNQ1 function

K69H-MinK subunits were studied with KCNQ1 to assess whether this site, analogous to R83H-MiRP2, was significant to function. Like wild-type MinK, K69H-MinK led to slow activation of KCNQ1-containing channels with depolarization (Fig. 7A). Conversely, K69H-MinK shifted the half-maximal activation to 50 ± 0.1 mV (without a significant change in slope) from 30 ± 0.8 mV as measured for wild-type MinK/KCNQ1 channels (Fig. 7B). The mean current passed by K69H-MinK/KCNQ1 channels was ~twofold lower than those with wild-type MinK at both 40 mV (2.7±0.2 vs. 5.4±0.1 μA at, *n*=14) and -80 mV (265±22 nA vs. 671±60 nA) (Fig. 7C). K69H-MinK/KCNQ1 channels showed faster deactivation kinetics with a mean time constant (τ) for deactivation of 277 ± 16 ms (-80 mV) vs. 827 ± 75 ms for wild-type complexes (Fig. 7D, E). Effects on KCNQ1 inactivation (25) were not evaluated.

R/K → H suppresses all KCNE effects on HERG whereas D → N impedes only up-regulation

MiRP1 assembles with HERG to pass currents with the attributes of cardiac I_{Kr} channels, and inherited variants of MiRP1 are associated with congenital long QT syndrome and drug-induced torsades de pointes (7, 13). MiRP1 mutations associated with disease reduce currents passed through channels formed with HERG by decreasing unitary conductance, shifting the $V_{1/2}$ of activation, speeding deactivation, and/or increasing sensitivity to drug blockade. HERG was studied here with K75H-MiRP1 and D82N-MiRP1, changes analogous to those associated with disease when carried in MiRP2 and MinK; then R83H-MiRP2 and D90N-MiRP2 were evaluated.

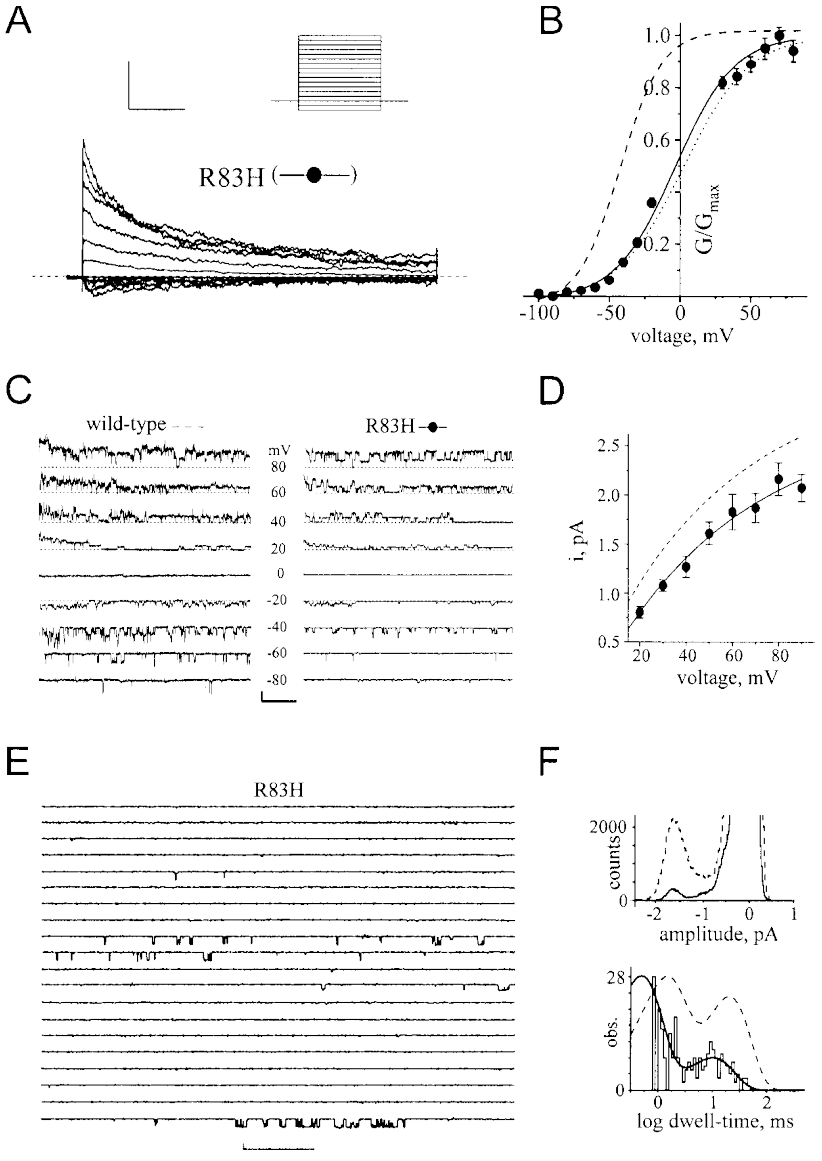

Figure 5. R83H-MiRP2/Kv3.4 complexes show altered voltage dependence, lower unitary current, and diminished open probability. Studies of R83H-MiRP2/Kv3.4 (filled circles) vs. wild-type MiRP2/ Kv3.4 (dashed line) and Kv3.4 (dotted line) performed in CHO cells in on-cell patches with 100 mM potassium solution in bath and pipette using protocol 1. Sampled 5 kHz, filtered at 1 kHz or 500 Hz. A) Representative R83H-MiRP2/Kv3.4 current family from a high channel density patch with holding voltage -80 mV, steps from -100 to 90 mV (inset, protocol 1); scale bars 50 pA and 500 ms; zero current level (dashed line). B) Normalized mean conductance-voltage relationship for patches as in panel A (n=9 –16 patches). Curves fit to a function of the form: $1/\{1+\exp[(V_{1/2}-V)/ V_s]\}$, where $V_{1/2}$ is the half-maximal voltage of activation and V_s the slope factor; values in text.; error bars indicate se. Dashed line shows results for wild-type MiRP2/Kv3.4 channels (Fig. 2); dotted line shows results for homomeric Kv3.4 channels as reported (8). C) Activation of ~5 R83H-MiRP2/Kv3.4 channels by steps from a holding voltage of -80 mV according to protocol 1. Scale bars, 2 pA and 1 s. D) Unitary current-voltage relationship calculated from all-points histograms constructed with > 2 x 10^5 events (>500 transitions) per patch for wild-type MiRP2/Kv3.4 (dashed line, ref 8) and R83H-MiRP2/Kv3.4 (solid line, filled circles); mean ± se for 4 –5 patches per point. E) Representative single-channel R83H-MiRP2/Kv3.4 steady-state currents at -40 mV; scale bars 1 pA and 500 ms (protocol 3). Traces (6 s per line) are continuous and taken from 5–10 min records. F) Upper panel: representative all-points histograms from steady-state wild-type MiRP2/Kv3.4 (dashed) and R83H-MiRP2/Kv3.4 (solid line) single-channels held at -40 mV for 5–10 min and indicative of Po. Lower panel: representative dwell-time histogram at -40 mV from a single R83H-MiRP2/Kv3.4 channel held at steady state for 5–10 min; fit to a double exponential function (solid line) using Marquardt least-squares (PSTAT). A double exponential function dwell-time fit for single wild-type MiRP2/Kv3.4 channels is shown for comparison (dashed line). Wild-type fits as reported (8); τ values in text.

The K75H mutation decreased the down-regulatory effects of MiRP1 on HERG. K75H-MiRP1/HERG complexes showed a mean tail current density of 2.5 ± 0.2 μA at -30 mV similar to HERG channels (3.1±0.1 μA) rather than wild-type MiRP1/HERG channels (0.76±0.1 μA, *n*=16 –20 cells) (Fig. 8A, left; B). Similarly, current deactivation with K75H-MiRP1 was like that of homomeric HERG channels (τ=838±85 and 970±72 ms at -100 mV, respectively) rather than wild-type MiRP1/HERG complexes (τ=221±8 ms) (Fig. 8A: right, C). Conversely, the D82N change did not interfere with the capacity of MiRP1 to reduce HERG currents or speed deactivation rates. D82N-MiRP1 channels showed a mean tail current density of 0.84 ± 0.1 μA (Fig. 8A, B) and a mean deactivation rate at -100 mV of 196 ± 7 ms (Fig. 8C), not significantly different from channels with wild-type MiRP1.

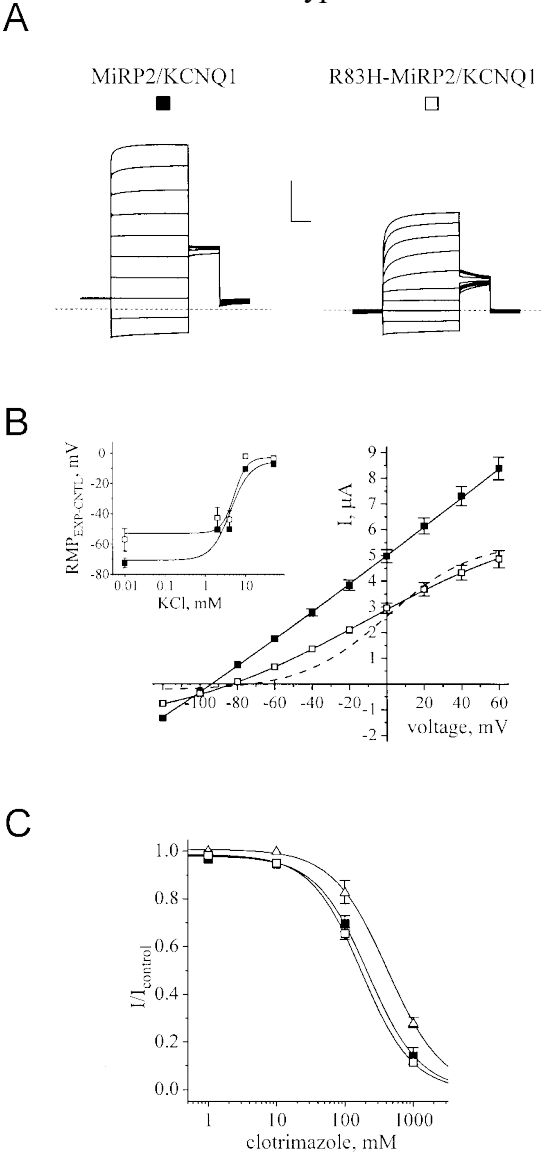

Figure 6. R83H-MiRP2/KCNQ1 complexes also show reduced current density and recovery of voltage and time dependence. Properties of channels formed with KCNQ1 (triangle), MiRP2/KCNQ1 (filled square), or R83H-MiRP2/KCNQ1 (open square) in oocytes studied by two-electrode voltage clamp. A) Representative current traces using protocol 4 in 4 mM potassium bath solution. Dashed line indicates zero current level; scale bars represent 2 mA and 1 s. B) Current-voltage relationships for cells as in panel A; mean ± SE for 16 –22 oocytes. Wild-type MiRP2/Kv3.4 fit with a straight line; R83H-MiRP2/Kv3.4 fit to a function of the form: $1/\{1+\exp[(V_{1/2}-V)/V_s]\}$, where $V_{1/2}$ is the half-maximal voltage of activation and V_s the slope factor. Dashed line with no symbols indicates KCNQ1 alone values for comparison. Inset: RMP studied as in panel C of Fig. 4; mean ± SE for 5– 8 oocytes. C) Clotrimazole dose-response for Kv3.4, wild-type MiRP2/Kv3.4 or R83H-MiRP2/Kv3.4 fit to the function: $y = [A_1-A_2/\{1+(x/x_o)^p\}] + A_2$, where x is added drug, x_o the inhibition constant, and p the Hill coefficient. Inhibition was assessed at 0 mV with various levels of drug in the bath and a repetitive pulse protocol (protocol 2); mean ± SE for 3–5 oocytes.

MiRP2 suppresses HERG currents in experimental cells by ~60% (Fig. 9A) as reported by Schroeder and colleagues (20). R83H-MiRP2 suppressed HERG much less efficiently (~20%): mean tail currents at -30 mV were 770 ± 140 nA for R83H-MiRP2/HERG channels, 320 ± 84 nA for channels with wild-type MiRP2, and 960 ± 54 nA for homomeric HERG channels (Fig. 9B). Just as D82N-MiRP1 influenced HERG like wild-type MiRP1 (Fig. 8), so D90N-MiRP2 suppressed HERG currents as efficiently as wild-type MiRP2: cells expressing D90N-MiRP2 and HERG showed mean tail currents of 330 ± 62 nA at -30 mV, an ~60% suppression current (Fig. 9B). Conversely, wild-type MinK has been shown to augment HERG currents by increasing the active fraction of channels in the membrane whereas D77N rat MinK (equivalent to D76N-human MinK) suppressed this up-regulatory effect despite its continued capacity to assemble with HERG (14, 24).

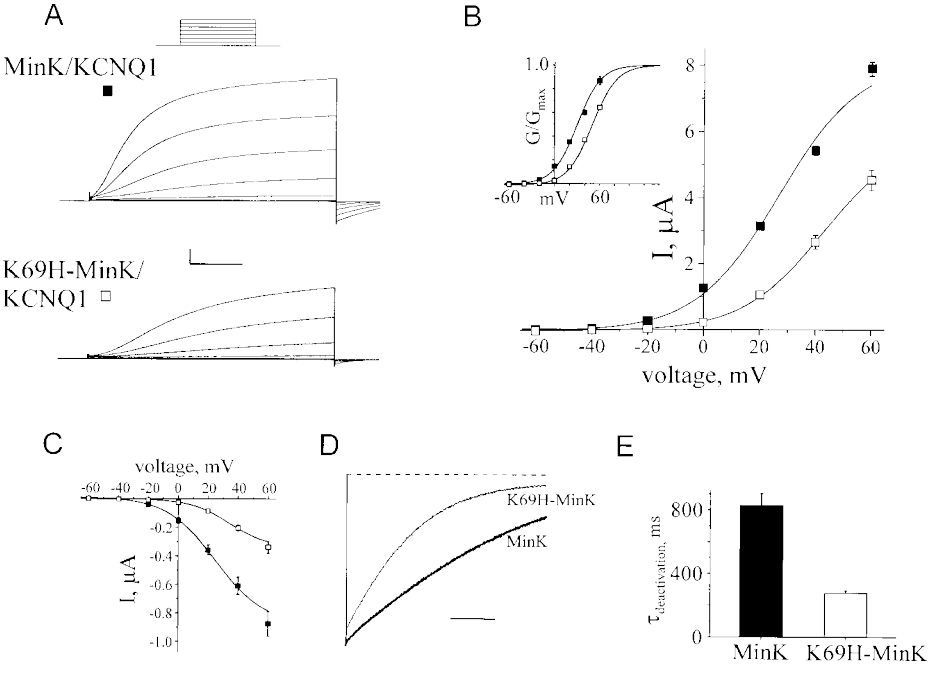

Figure 7. K69H-MinK/KCNQ1 complexes show altered voltage dependence speeded deactivation and reduced potassium flux. Channels formed with wild-type MinK/ KCNQ1 (filled square) or K69H-MinK/KCNQ1 (open square) in oocytes studied by two-electrode voltage clamp. A) Representative current traces with protocol 5 (in-set) in 4 mM bath potassium solution. Scale bars, 1 µA and 1 s. B) Current-voltage relationships for cells as in panel A; mean ± $_{SE}$ for 14 oocytes. Curves fit to a function of the form: $1/\{1+\exp[(V_{1/2}-V)/V_s]\}$, where $V_{1/2}$ is the half-maximal voltage of activation and V_s the slope factor. Inset: normalized conductance-voltage relationship. C) Tail current-voltage relationships for panel B. D) Normalized tail currents at -80 mV with a prepulse to 40 mV for wild-type MinK/ KCNQ1 (boldface) or K69H-MinK/KCNQ1 (thin). Scale bar represents 200 ms. E) Deactivation rates from tail currents as in panel D; fit to a single exponential; mean ± $_{SE}$ for 7 oocytes in each group.

DISCUSSION

Common effects of conserved sites in different MiRP/a subunit complexes

Two conserved residues have been studied to assess how KCNE peptides (MiRPs) alter α subunit function and to determine whether these sites influence different α subunits similarly. The sites were chosen because their inheritance in mutant form has been associated with disease and altered channel function. Mutation of these residues in MinK, MiRP1, or MiRP2 was found to have similar effects in channels formed with KCNQ1 or Kv3.4. Each wild-type MiRP acted with these α subunits to increase potassium current, and both D→ N changes (MinK-76, MiRP1– 82, and MiRP2–90) and R/K→ H changes (MinK-69, MiRP1–75, and MiRP2– 83) disrupted this capacity to increase flux. Like arrhythmia-associated D76N-MinK with KCNQ1 (12), D90N-MiRP2 shifted activation of Kv3.4 channels to more depolarized potentials, diminished steady-state open probability, lowered unitary conductance, and altered the voltage dependence KCNQ1 channels to

diminish current density. Like periodic paralysis-associated R83H-MiRP2 with Kv3.4 (8), R83H-MiRP2 and K69H-MinK decreased current through KCNQ1 channels due to a shift in activation to more depolarized potentials.

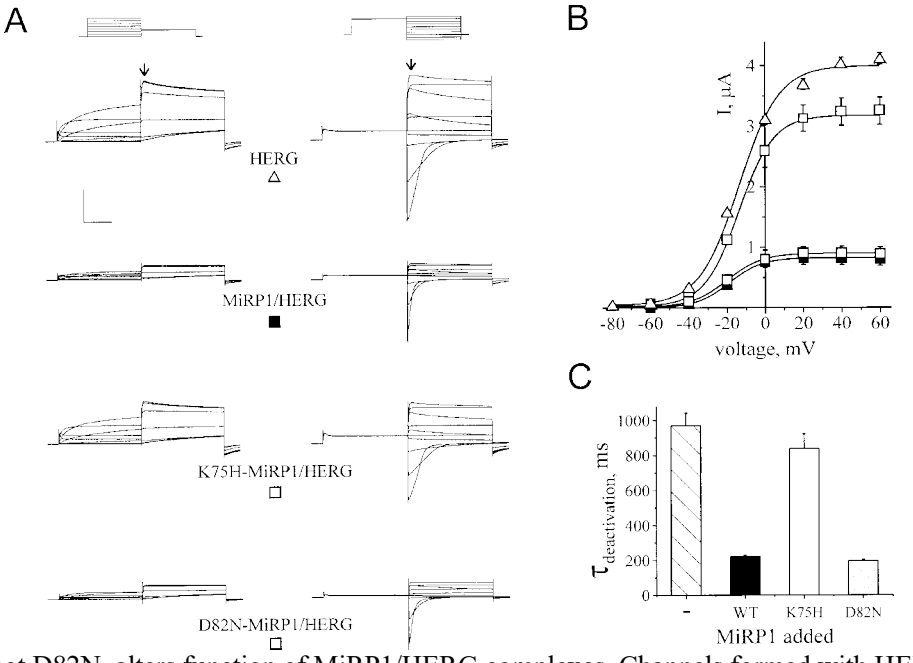

Figure 8. K75H, but not D82N, alters function of MiRP1/HERG complexes. Channels formed with HERG (triangle), wild-type MiRP1/HERG (filled square), K75H-MiRP1/HERG (open square), or D82N-MiRP1/HERG (gray square) in oocytes studied by two-electrode voltage clamp. A) Left panels. Currents with a varied prepulse voltage and a -30 mV tail (protocol 6, inset). Right panels: 40 mV prepulse with varied tail test voltage (protocol 7, inset). Bath solution was 4 mM potassium solution. Scale bars represent 1 μA and1 s. B) Current-voltage relationships for cells as in panel A (left) measured at arrow; mean ± SE for 16 –20 oocytes. Curves fit to a function of the form: $1/\{1+\exp[(V_{1/2}-V)/V_s]\}$, where $V_{1/2}$ is the half-maximal voltage of activation and V_s the slope factor. C) Deactivation rates at -100 mV as in panel A (right); fit to a single exponential; mean ± SE for 7– 8 oocytes; HERG (hatched); wild-type MiRP1/HERG (black); K75H-MiRP1/HERG (open); D82N-MiRP1/HERG (gray).

HERG α subunits are stimulated by assembly with MinK and suppressed by MiRP1 and MiRP2 (14, 20) and the two conserved residues exhibited differential effects on these regulatory events. Whereas stimulation of HERG was impeded by D77N mutation in rat minK (14), D82N-MiRP1 and D90N-MiRP2 suppressed activity like wild-type subunits. Conversely, K75H-MiRP1 and R83H-MiRP2 suppressed HERG less effectively than did wild-type.

Thus, R/K→ H mutation disrupted the ability of all three KCNE peptides to alter α subunit function whether the wild-type effect was to increase or suppress current. This residue appears to be important for normal MiRP function. Whereas D→ N mutation disabled the ability of the MinK to increase potassium flux, it did not alter MiRP1 or MiRP2 suppression of HERG, suggesting either a more specific role for this residue or that the unique attributes of HERG yield this behavior. These effects of KCNE peptide mutations indicate their operation by common mechanisms and shared structures.

Sites of contact between MiRPs and α subunits remain to be identified. Studies using mutagenesis, modification, pharmacology, electrophysiology, and antibody binding have revealed that KCNE peptides are type I transmembrane proteins that appear to cross the membrane in proximity to the channel pore (2, 7, 8, 22, 26). The effects of disease-associated mutations support a general correlation of function and domain: mutations in the extracellular region of MiRP1 alter voltage-dependent activation and drug blockade (T8A and Q9E) (7, 13); mutations in the transmembrane and membrane-following segments influence gating kinetics and ion conduction (7–9, 12). Indeed, transplantation of residues 57–59 from the transmembrane segment of MinK to the equivalent sites in MiRP2 was sufficient to convert MiRP2/KCNQ1 channels from leak-type conductances to slowly activating MinK/ KCNQ1-like channels (19). The two sites studied here

reside in the membrane-following region, and their potent influence on gating and pore function suggests an interaction with α subunit S4, S5, and/or S6 segments (27, 28).

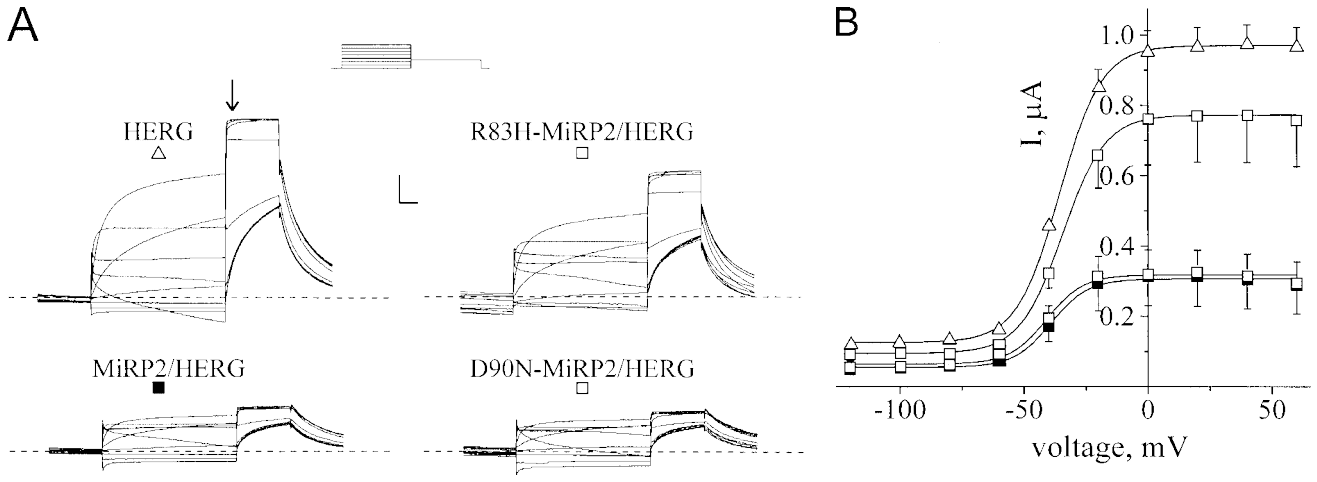

Figure 9. R83H, but not D90N, alters function of MiRP2/HERG complexes. Channels formed with HERG (triangle), wild-type-MiRP2/HERG (filled square), R83H-MiRP2/HERG (open square), or D90N-MiRP2/HERG (gray square) in oocytes studied by two-electrode voltage clamp. A) Currents with varied prepulse voltage and a -30 mV tail (protocol 7, inset). Bath solution was 4 mM potassium solution. Scale bars represent 1 μA and1 s. B) Current-voltage relationships for cells as in panel A (arrow); mean ± SE for 18 – 40 oocytes. Curves fit to a function of the form: $1/\{1+\exp[(V_{1/2}-V)/V_s]\}$, where $V_{1/2}$ is the half-maximal voltage of activation and V_s the slope factor.

Promiscuous interactions: a role in disease?

We hypothesize here that interaction of MiRPs with a variety of α subunits and the capacity of MiRP mutations to alter function in the different complexes contribute to the varied clinical manifestations of MiRP-associated disease. Although the idea is appealing in its simplicity, proof for the hypothesis remains scant. A multiplicity of MIRP/α subunit interactions has been suggested by studies of cloned subunits in experimental cells, but in only a few cases has a direct comparison of cloned and native currents, transcript and/or protein expression, and/or linkage to human disease provided strong support for native assembly; these include MinK with KCNQ1 in heart and inner ear, MiRP1 with HERG in the heart, and MiRP2 with Kv3.4 in skeletal muscle (5– 8, 29, 30).

Indeed, there is no compelling need to invoke promiscuous interactions in described KCNE-associated disorders. Cardiac arrhythmia and deafness in association with MinK mutations can be fully rationalized by diminished function of MinK/KCNQ1 channels in both the heart and ear (29, 31–33). MiRP1 mutations associated with a prolonged QT interval at baseline (Q9E, M54T, I57T, and A116V) act as one might expect to reduce currents passed through channels formed with HERG (by decreasing unitary conductance, shifting the voltage dependence of activation, and/or speeding of deactivation, thereby slowing cardiac repolarization) (7, 13). These rare mutations create a substrate for a poor response to further current suppression by drugs known to block cardiac potassium channels (13). More specific effects are observed with one rare mutation (Q9E) and a common polymorphism (T8A) linked to antibiotic-induced arrhythmia, as these MiRP1 variants increase sensitivity of MiRP1/ HERG channels to blockade by the inciting drugs (7, 13). Finally, R83H-MiRP2 is associated with periodic paralysis and alters both the attributes of a prominent skeletal muscle cell potassium current and the resting membrane potential of muscle cells via endogenous MiRP2/Kv3.4 channels (8).

Other observations remain controversial. We reported association of MiRP1 mutations with cardiac arrhythmias (inherited and drug-induced) and altered function of MiRP1/HERG channels (7, 13); others have subsequently suggested that MiRP1 interaction with KCNQ1 (34), HCN1 (18), or Kv4.2 (17) might instead produce abnormal cardiac rhythms. So far we have been unable to demonstrate an effect of MiRP1 on KCNQ1 or HCN1 currents in either oocytes or CHO cells; evidence for these interactions may require

specific experimental conditions. We do observe MiRP1 to alter Kv4.2 subunit function (16), but suspect that this influences the central nervous system in humans rather than the heart as Kv4.2 transcript is abundant in the brain but appears to be absent from human heart (35). Similarly, patients with periodic paralysis in association with MiRP2 mutation show abnormal skeletal muscle cell function reflective of altered MiRP2/Kv3.4 channel activity (8); others speculate that the primary role for MiRP2 is with KCNQ1 in the colon (based on transcript expression patterns) (20). Although notable effects of MiRP2 on KCNQ1 are reproduced here, individuals with MiRP2-associated periodic paralysis did not show abnormal gastrointestinal function (8) as might be expected if MiRP2/KCNQ1 complexes were central to fluid handling in the colon (20). Moreover, two probes used to demonstrate abundant transcript for MiRP2 in human skeletal muscle failed to visualize mRNA in the colon (8). Finally, we could not recapitulate MiRP2 suppression of KCNQ4 currents (20) when the two subunits were coexpressed in oocytes (not shown).

Why, then, hypothesize a role for promiscuous interaction? First, there is marked variation among recognized cases of KCNE-associated disease in clinical presentation, response to medical intervention, and long-term outcome, which may reflect such additional MinK, MiRP1, or MiRP2 interactions. Second, function of KCNE peptides with multiple α subunit types might be difficult to discern if assembly takes place only in some cell types or under unique circumstances; indeed, cardiac potassium channel α subunits show spatial and temporal variation in expression during development and in disease (36). Finally, it is the very capacity of KCNE peptides to operate with different α subunits in experimental cells that impels consideration of the hypothesis that the interactions occur in nature. Proof requires discovery of a KCNE mutation that yields pathology due to its aberrant function in more than one channel type.

This work was supported by a National Institutes of Health grant to S.A.N.G. We are grateful to M. Buck, L. Kim, and D. Goldstein for expert technical assistance.

REFERENCES

1. Hille, B. (1992) *Ionic Channels of Excitable Membranes*, Sinauer, Sunderland, MA
2. Abbott, G. W., and Goldstein, S. A. N. (1998) A superfamily of small potassium channel subunits: form and function of the MinK-related peptides (MiRPs). *Q. Rev. Biophys*. **31**, 357–398
3. Abbott, G. W., and Goldstein, S. A. N. (2001) Potassium channel subunits encoded by the KCNE gene family: physiology and pathophysiology of the MinK-related peptides (MiRPs). *Mol. Interventions* **1**, 95–107
4. Takumi, T., Ohkubo, H., and Nakanishi, S. (1988) Cloning of a membrane protein that induces a slow voltage-gated potassium current. *Science* **242**, 1042–1045
5. Barhanin, J., Lesage, F., Guillemare, E., Fink, M., Lazdunski, M., and Romey, G. (1996) K(V)LQT1 and IsK (minK) proteins associate to form the I(Ks) cardiac potassium current. *Nature (London)* **384**, 78 – 80
6. Sanguinetti, M. C., Curran, M. E., Zou, A., Shen, J., Spector, P. S., Atkinson, D. L., and Keating, M. T. (1996) Coassembly of K(V)Lqt1 and Mink (Isk) proteins to form cardiac I-Ks potassium channel. *Nature (London)* **384**, 80 – 83
7. Abbott, G. W., Sesti, F., Splawski, I., Buck, M., Lehmann, M. H., Timothy, K. W., Keating, M. T., and Goldstein, S. A. N. (1999) MiRP1 forms IKr potassium channels with HERG and is associated with cardiac arrhythmia. *Cell* **97**, 175–187
8. Abbott, G. W., Butler, M. H., Bendahhou, S., Dalakas, M. C., Ptacek, L. J., and Goldstein, S. A. N. (2001) MiRP2 forms potassium channels in skeletal muscle with Kv3.4 and is associated with periodic paralysis. *Cell* **104**, 217–231
9. Splawski, I., Tristani-Firouzi, M., Lehmann, M. H., Sanguinetti, M. C., and Keating, M. T. (1997) Mutations in the hminK gene cause long QT syndrome and suppress IKs function. *Nat. Genet*. **17**, 338 –340
10. Schulze-Bahr, E., Wang, Q., Wedekind, H., Haverkamp, W., Chen, Q., and Sun, Y. (1997) KCNE1 mutations cause Jervell and Lange-Nielsen syndrome. *Nat. Genet*. **17**, 267–268

11. Duggal, P., Vesely, M. R., Wattanasirichaigoon, D., Villafane, J., Kaushik, V., and Beggs, A. H. (1998) Mutation of the gene for IsK associated with both Jervell and Lange-Nielsen and Romano-Ward forms of long-QT syndrome. *Circulation* **97**, 142–146
12. Sesti, F., and Goldstein, S. A. N. (1998) Single-channel characteristics of wildtype IKs channels and channels formed with two minK mutants that cause long QT syndrome. *J. Gen. Phys*. **112**, 651– 664
13. Sesti, F., Abbott, G. W., Wei, J., Murray, K. T., Saksena, S., Schwartz, P. J., G., P. S., Roden, D. M., George, A. L. J., and Goldstein, S. A. N. (2000) A common polymorphism associated with antibiotic-induced cardiac arrhythmia. *Proc. Natl. Acad. Sci. USA* **97**, 10613–10618
14. McDonald, T. V., Yu, Z., Ming, Z., Palma, E., Meyers, M. B., Wang, K. W., Goldstein, S. A. N., and Fishman, G. I. (1997) A minK-HERG complex regulates the cardiac potassium current IKr. *Nature (London)* **388**, 289 –292
15. Tapper, A. R., and George, A. L. (2000) MinK subdomains that mediate modulation of and association with KvLQT1. *J. Gen. Physiol.* **116**, 379 –389
16. Kim, L. A., Abbott, G. W., Butler, M. H., and Goldstein, S. A. N. (2001) A role for MiRP1-Kv4.2 in CNS A-type currents? *Biophys. J.* **80**, 437a
17. Zhang, M., Jiang, M., and Tseng, G. (2001) MiRP1 associates with Kv4.2 and modulates its gating function. A potential role as (3 subunit of cardiac transient outward channel? *Circ. Res*. **88**, 1012–1019
18. Yu, H., Wu, J., Potapova, I., Wymore, R. T., Holmes, B., Zuckerman, J., Pan, Z., Wang, H., Shi, W., Robinson, R. B., El-Maghrabi, M. R., Benjamin, W., Dixon, J., McKinnon, D., Cohen, I. S., and Wymore, R. (2001) MinK-related peptide 1: a beta subunit for the HCN ion channel subunit family enhances expression and speeds activation. *Circ. Res*. **88**, E84 – 87
19. Melman, Y. F., Domenech, A., de la Luna, S., and McDonald, T. V. (2001) Structural determinants of KvLQT1 control by the KCNE family of proteins. *J. Biol. Chem*. **276**, 6439 – 6444
20. Schroeder, B. C., Waldegger, S., Fehr, S., Bleich, M., Warth, R., Greger, R., and Jentsch, T. J. (2000) A constitutively open potassium channel formed by KCNQ1 and KCNE3. *Nature (London)* **403**, 196 –199
21. Abbott, G. W., Goldstein, S. A. N., and Sesti, F. (2001) Do all voltage-gated potassium channels use MiRPs? *Circ. Res*. **88**, 981–983
22. Wang, K. W., and Goldstein, S. A. N. (1995) Subunit composition of minK potassium channels. *Neuron* **14**, 1303–1309
23. Bockenhauer, D., Zilberberg, N., and Goldstein, S. A. N. (2001) KCNK2: reversible conversion of a hippocampal potassium leak into a voltage-dependent channel. *Nature Neurosci*. **4**, 486 – 491
24. Bianchi, L., Shen, Z., Dennis, A. T., Priori, S. G., Napolitano, C., Ronchetti, E., Bryskin, R., Schwartz, P. J., and Brown, A. M. (1999) Cellular dysfunction of LQT5-minK mutants: abnormalities of IKs. IKr and trafficking in long QT syndrome. *Hum. Mol. Genet*. **8**, 1499 –1507
25. Tristani-Firouzi, M., and Sanguinetti, M. C. (1998) Voltage-dependent inactivation of the human K+ channel KvLQT1 is eliminated by association with minimal K+ channel (minK) subunits. *J. Physiol. (London)* **510**, 37– 45
26. Tai, K. K., and Goldstein, S. A. N. (1998) The conduction pore of a cardiac potassium channel. *Nature (London)* **391**, 605– 608
27. Franqueza, L., Lin, M., Shen, J., Splawski, I., Keating, M. T., and Sanguinetti, M. C. (1999) Long QT syndrome-associated mutations in the S4 –S5 linker of KvLQT1 potassium channels modify gating and interaction with minK subunits. *J. Biol. Chem.* **274**, 21063–21070
28. del Camino, D., Holmgren, M., Liu, Y., and Yellen, G. (2000) Blocker protection in the pore of a voltage-gated K+ channel and its structural implications. *Nature (London)* **403**, 321–325
29. Vetter, D. E., Mann, J. R., Wangemann, P., Liu, J., McLaughlin, K. J., Lesage, F., Marcus, D. C., Lazdunski, M., Heinemann, S. F., and Barhanin, J. (1996) Inner ear defects induced by null mutation of the *IsK* gene. *Neuron* **17**, 1251–1264
30. Franco, D., Demolombe, S., Kupershmidt, S., Dumaine, R., Dominguez, J. N., Roden, D., Antzelevitch, C., Escande, D., and Moorman, A. F. M. (2001) Divergent expression of delayed

rectifier K+ channel subunits during mouse heart development. *Cardiovasc. Res*. **52**, 65–75
31. Kaczmarek, L. K., and Blumenthal, E. M. (1997) Properties and regulation of the minK potassium channel protein. *Physiol. Rev*. **77**, 627– 641
32. Ackerman, M. J. (1998) The long QT syndrome: ion channel diseases of the heart. *Mayo Clin. Proc*. **73**, 250 –269
33. Sanguinetti, M. C. (2000) Long QT syndrome: ionic basis and arrhythmia mechanism in long QT syndrome type 1. *J. Cardiovasc. Electrophysiol.* **11**, 710 –712
34. Tinel, N., Diochot, S., Borsotto, M., Lazdunski, M., and Barhanin, J. (2000) KCNE2 confers background current characteristics to the cardiac KCNQ1 potassium channel. *EMBO J*. **19**, 6326 – 6330
35. Zhu, X. R., Wulf, A., Schwarz, M., Isbrandt, D., and Pongs, O. (1999) Characterization of human Kv4.2 mediating a rapidly-inactivating transient voltage-sensitive K+ current. *Recept. Channels* **6**, 387– 400
36. Nerbonne, J. M. (1998) Regulation of voltage-gated K+ channel expression in the developing mammalian myocardium. *J. Neurobiol.* **37**, 37–59

Received for publication June 25, 2001.
Revised for publication November 27, 2001.